Unsupervised Deep Anomaly Detection for Medical Images Using an Improved Adversarial Autoencoder

Haibo Zhang[1] · Wenping Guo[1,2] · Shiqing Zhang[1] · Hongsheng Lu[1] · Xiaoming Zhao[1]

Abstract

Anomaly detection has been applied in the various disease of medical practice, such as breast cancer, retinal, lung lesion, and skin disease. However, in real-world anomaly detection, there exist a large number of healthy samples, and but very few sick samples. To alleviate the problem of data imbalance in anomaly detection, this paper proposes an unsupervised learning method for deep anomaly detection based on an improved adversarial autoencoder, in which a module called chain of convolutional block (CCB) is employed instead of the conventional skip-connections used in adversarial autoencoder. Such CCB connections provide considerable advantages via direct connections, not only preserving both global and local information but also alleviating the problem of semantic disparity between the encoding features and the corresponding decoding features. The proposed method is thus able to capture the distribution of normal samples within both image space and latent vector space. By means of minimizing the reconstruction error within both spaces during training phase, higher reconstruction error during test phase is indicative of an anomaly. Our method is trained only on the healthy persons in order to learn the distribution of normal samples and can detect sick samples based on high deviation from the distribution of normality in an unsupervised way. Experimental results for multiple datasets from different fields demonstrate that the proposed method yields superior performance to state-of-the-art methods.

Keywords Deep anomaly detection · Medical images · Unsupervised · Adversarial autoencoders · Chain of convolution block

Introduction

With the rapid advancement of computer technology, medical imaging plays a key role in the diagnosis, and identification of malignant lesions on medical image early and accurately will help to improve the followed treatment [1–7]. Among them, anomaly detection is one of the most significant challenging problems and aims to find outliers within the distribution of normal data. Nowadays, anomaly detection has been applied in the various disease of medical practice, including the areas of breast cancer, retinal, lung lesion, brain MRI, and skin disease [8–13]. However, the available data for real-world anomaly detection is highly imbalanced, and there is a large number of healthy samples, but very few sick samples. Such data imbalance hence limits the use of supervised learning methods. To alleviate this problem, unsupervised learning methods may provide a possible solution. This is because unsupervised learning methods can be trained only on normal data to capture the normality distribution, and then identifying the abnormal samples with high deviation from the distribution of normality.

At present, a considerable number of approaches have been proposed to detect anomalies. For instance, one-class support vector machine (OCSVM) is considered as an outstanding one. Linear OCSVM proposed by Erfani et al. [14], as an extension of OCSVM, was used for high-dimensional and large-scale anomaly detection. However, OCSVM is just used for classification tasks, rather than feature learning of medical imaging.

In recent years, anomaly detection based on unsupervised learning has been an active research subject. So far, a

✉ Hongsheng Lu
  luhs@tzc.edu.cn

✉ Xiaoming Zhao
  tzxyzxm@163.com

1 Taizhou Central Hospital (Taizhou University Hospital), Taizhou University, Zhejiang 318000, China

2 College of Computer and Information, Hohai University, Nanjing 210098, China

considerable number of methods have been proposed to detect the outlier samples. For instance, Akcay et al. [15] uses a new deep learning architecture called U-Net with skip connections for anomaly detection via adversarial training. However, this work empirically illustrates the semantic gap between the encoding features and the corresponding decoding features in U-Net with skip connections, thereby further hindering the improvement of reconstructing performance [16].

In order to address this issue, a new method for anomaly detection based on an improved adversarial autoencoder is proposed in this paper. Our method proposes to employ a chain of convolutional block (CCB) to replace the conventional skip-connections used in adversarial autoencoders. The used non-linear transformations in CCBs are able to bridge the semantic gap to some extent between the encoding features and the corresponding decoding features. Evaluation of our approach on typical cifar-10 dataset shows the proposed method achieves better performance than prior works [15, 17, 18]. Another evaluation on anomaly detection datasets, such as ILD [19] and HAM10000 [20], shows that the proposed method is a universal approach for medical image diagnosis, demonstrating its effectiveness.

The main contributions of this paper are summarized as follows:

1. An improved adversarial autoencoder is proposed for unsupervised deep anomaly detection from medical images. Specially, a new convolution module called chain of convolutional block (CCB) is employed instead of the conventional skip-connections used in adversarial autoencoders, which produces an improved adversarial autoencoder. The CCB module uses non-linear transformations to bridge the semantic gap to some extent between the encoding features and the corresponding decoding features.
2. The proposed method is evaluated on multiple datasets such as cifar-10, ILD, HAM10000, showing that our method yields superior performance to state-of-the-art methods.

The remainder of this paper is organized as follows: Related work is given in "Related Work" The proposed method using an improved adversarial autoencoder is provided in "Materials and Methods." In "Results and Analysis," we present the experiment results and finally give the conclusions in "Conclusion."

Related Work

Recently, anomaly detection based on unsupervised deep learning has been an emerging research subject, and a considerable number of methods have been explored to detect the anormal samples [8, 9, 21].

An autoencoder (AE) is one popular category of unsupervised deep learning. Cowton et al. [22] designed an autoencoder-based method, which is composed of gated recurrent units (GRUs) to deal with environmental sensor data, for monitoring respiratory disease of growing pigs. Petrick et al. [23] proposed a 3D convolutional autoencoder to detect disorders in emergency head CT, in which 11 layers of convolution blocks and 6 layers of deconvolution blocks are included. The results of evaluation show that this method has potentialities for anomaly detection in emergency head CT.

Different from the classical AE, variational autoencoder (VAE) [24] employed regularization on the manifolds structure, and it was trained with noise injected in the latent vector. Gunduz [25] took advantage of the VAE method as a feature extractor and the Relief-Fisher Score as a filter-based feature selector. This method had been validated on Parkinson's disease classification.

However, the above-mentioned methods based on the AE architecture are limited in modelling high-dimensional distributions, resulting in blurry reconstructions, large computation complexity, and inaccurate performance [26]. To alleviate this problem, adversarial AE, also known as Generative Adversarial Networks (GANs) [27], may provide a feasible solution.

Fujioka et al. [10] proposed a bidirectional GAN method to map input samples to a latent space during training, then defined an anomaly score using a convex combination of reconstruction and discriminator loss to detect anomaly samples. Schlegl et al. [28] hypothesized that the difference in the latent vector would generate anomalies and therefore trained a GAN to create a mapping between high-dimensional feature maps and low-dimensional latent feature maps. Such GAN-based model shows a clear improvement in comparison with previous methods such as Deep Convolutional GAN (DCGAN) [29]. However, the main drawback of this approach is that it has large computational complexity. Sabokrou et al. [30] supposed that the pre-trained GAN could not produce abnormal images, and the difference in image space would yield anomalies. Therefore, they proposed a new architecture with two modules, a reconstructor that learns the underlying concept of the target class, and a discriminator that works as the anomaly detector.

Akcay et al. [15, 17] emphasized that the high-dimensional image space was as important as low-dimensional latent space. In this case, they proposed an encoder-decoder-encoder model to capture the distribution of the image and latent space, and minimize the distance not only between the original and generated images, but also within their latent space representations [15]. Such anomaly detection approach achieved better performance and illustrated the importance of representations within the dual image and

latent space. In addition, Akcay et al. proposed another anomaly detection approach that utilizes a skip-connected adversarial autoencoder network architecture, reporting numerically superior performance to prior work such as GANomaly [17].

The U-Net architecture [31], proposed by Ronneberger et al. in 2015, has good image segmentation effect and scalability, since the network is symmetric consisting of an encoder and a decoder. The encoder extracts latent vector from input images, and the decoder reconstructs the segmentation maps from the latent vector. To improve the accuracy of image segmentation, Zongwei et al. presented a more powerful architecture, named UNet + + [32]. This architecture is essentially an encoder-decoder network where corresponding layers are connected through dense skip pathways, thereby reducing the semantic gap between the encoder and decoder sub-networks. With the help of redesigned skip pathways and deep supervision, the optimizer of the architecture deals with the learning task easily. However, Ibtehaz et al. empirically illustrated the encoding features, and the corresponding decoding features in a U-Net with skip connections could reduce the reconstructing performance [15, 16].

To address this issue, MultiResUNet [16], as an enhanced version of U-Net architecture, was developed to significantly advance the models of biomedical image segmentation. This architecture adopted residual paths to make the feature maps between the corresponding encoder-decoder layers more homogeneous. Furthermore, MultiRes, as a compact analogous structure to Inception blocks, was proposed to augment the ability of multi-resolution analysis of U-Net, but demanded less memory.

Considering the shortcoming of skip connections, this paper proposes to employ a chain of convolutional block (CCB) to replace the conventional skip-connections used in adversarial autoencoders, thereby producing a new method based on an improved adversarial autoencoder for deep anomaly detection.

Materials and Methods

In this section, we initially introduce the problem definition as well as the general framework of the proposed model. Then, we present the technical details and several key design issues.

Problem Definition

The dataset in our study is divided into a train set $D_{train} = \{X, y\}_{i=1}^{m}$ and a test set $D_{test} = \{X, y\}_{i=1}^{n}$. The train set is composed of only normal image, and the test set contains both normal and abnormal images. In a practical setting, the number of the train set m is much larger than number of the test set n.

According to the data setting defined above, a model M and a scoring function $A(.)$ were trained on the images from normal classes. The model M is trained to capture the distribution of D_{train} to reconstruct the output $\hat{x}$, and map input image x and output $\hat{x}$, into the hidden latent vector z and $\hat{z}$. The scoring function $A(.)$ defined on $(x, \hat{x}, z, \hat{z})$ would yield the minimum score for normal samples, but higher score for abnormal samples, as expressed in Eqs. (1), (2) and (3):

$$\hat{x}, z, \hat{z} = M(x) \tag{1}$$

$$A(\cdot) = \alpha \cdot D_1(x, \hat{x}) + (1 - \alpha)D_2(z, \hat{z}) \tag{2}$$

$$f(x) = \begin{cases} 0 & A(x) < \phi \\ 1 & A(x) > \phi \end{cases} \tag{3}$$

Proposed Method

Figure 1 illustrates the overview of the proposed method, in which a generator networks G as well as a discriminator networks D are included. The generator networks G employ a shamrock network with an encoder G_E, a chain of convolution block (CCB), and a decoder G_D sub-network. The encoder network G_E maps input image x into the latent vector z, and the decoder network G_D reconstructs the output image $\hat{x}$ from z. Here, the decoder G_D adopts a CCB as skip-connection approach such that the encoding features are passed through a CCB, and then concatenate with the decoding feature. Here, the CCB is used to alleviate the disparity between the encoding and decoding features.

The discriminator network D is not only used as a classifier but also as a feature extractor. The task of classifier is to classify input image x from the reconstructed image $\hat{x}$, while the task of feature extractor is to compute latent representations of input image and reconstructed image.

The objective function of training this network M is to minimize three loss functions: similarity loss L_s, adversarial loss L_{adv}, and latent loss L_{lat}. Both similarity loss and adversarial loss are used to maximize the reconstruction capability; however, the adversarial loss proposed in this work imposes the network to generate realistic images, while the similarity loss ensures the generated image similar to the normal images [27]. The similarity loss and adversarial loss are separately shown:

$$L_{adv} = \underset{x \sim p_x}{E}(\log(D(x))) + \underset{x \sim p_x}{E}\left(\log\left(1 - D(\hat{x})\right)\right) \tag{4}$$
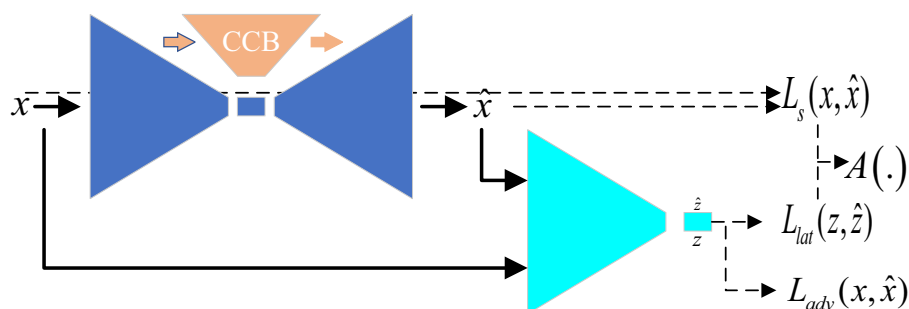
Fig. 1 The overview of the proposed method. It comprises a generator G and a discriminator D. The generator G employs a shamrock network with an encoder G_E, a chain of convolution block (CCB), and a decoder G_D sub-network. A CCB works as a skip-connection approach to alleviate the disparity between the encoding and decoding features

$$L_s = \underset{x \sim p_x}{E} |x - \hat{x}|_2 \tag{5}$$

Owing to using the adversarial and similarity losses, the network is capable of reconstructing realistic and similar images. As explained in "Introduction," it is needed to guarantee to generate latent vector for input image and reconstructed image as similar as possible. The latent loss is defined as

$$L_{lat} = \underset{x \sim p_x}{E} |z - \hat{z}|_2 \tag{6}$$

With the three loss functions defined above, the total training objective function is rewritten as:

$$L = \min(\lambda_s L_s + \lambda_{adv} L_{adv} + \lambda_{lat} L_{lat}) \tag{7}$$

CCB

As shown in Fig. 2, a chain of convolution (CCB) contains a line of convolution (conv.) block, and the length of the line depends on the depth of the encoder and decoder layers. The length of a CCB for shallow layer is long; otherwise, it is short. The used convolution block contains a 3×3 CNN layer. And it is followed by a ReLU layer with a filter 3×3, making the output feature maps have the same size. Such architecture is proven to be efficient in medical image classification [33]. Note that such CCB connections provide considerable advantages via direct connections, not only preserving both global and local information but also alleviating the problem of semantic disparity between the encoder features and the corresponding decoder features.

Details of The Sub-network Architecture

As showed in Fig. 3, the encoder network G_E has 5 downsample blocks which are composed of a CNN layer, a BN layer, and a LeakyReLU activation layer. The G_E captures the distribution of input image space and maps high-dimensional input image features into a low-dimensional latent feature representation. Symmetrically, the network G_D also contains 5 blocks and up-samples the low-dimensional latent feature representation back to high-dimensional feature representation. The network G_D utilizes skip-connection strategy with CCBs, so that each layer in the network G_E and the corresponding layer in G_D is connected by CCBs.

Results and Analysis

In this section, the task setting, the evaluation criteria, and datasets were firstly provided. Then, the results were analyzed.
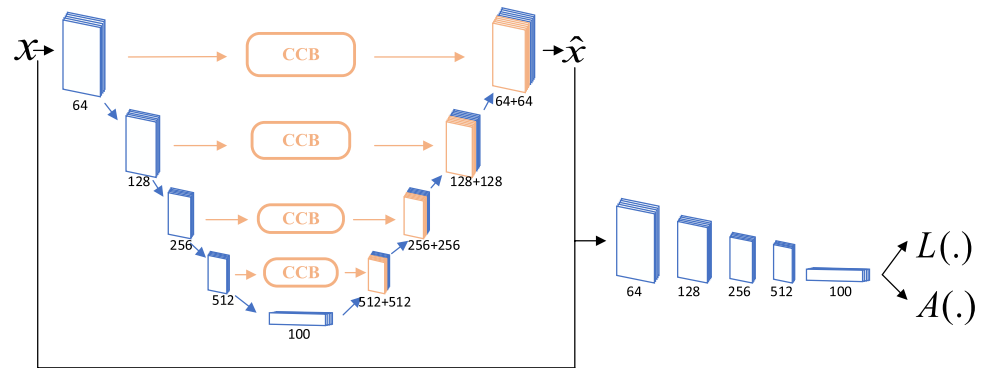
Experimental Setup

Task Setting

Task1: we compare the proposed method with prior works on image classification tasks.

Task2: we evaluate the performance of the proposed method in medical image diagnosis.

Fig. 2 The architecture of a chain of convolution block (CCB). A CCB contains a line of convolution (conv.) block, and the length of the line depends on the depth of the encoder and decoder layers

Fig. 3 Details of the sub-network architecture. The network has 5 layers, and each layer in network G_E and the corresponding layer in G_D is connected by CCBs

Task3: we discuss the effect of different lengths of CCBs on classification performance.

Evaluation Criteria

The area under the curve (AUC) method was used for performance evaluation in Task 1 in order to compare the proposed method with prior works using the same criteria as used in [15]. However, the model evaluation of experiments is a one-class classification task, which is needed to assign a hard label to a given sample. As a result, we also adopted "Accuracy" and "F1 score" to evaluate the performance of the proposed method in Task 2 as done in [34].

Accuracy is adopted as a statistical indicator of performance measure. This indicator is used to describe how well a binary classification test correctly recognizes or excludes a condition. In other words, the accuracy represents the percentage of correctly predicted ones in the total samples.

Precision refers to as positive predictive value and denotes the probability of truly positive ones among all the positive samples.

Recall refers to the true positive rate or sensitivity, which means the probability of true positive among all the true samples.

F1-score is a measure indicator of a test's accuracy and represents the harmonic average values of the precision and the recall. The optimal value of F1-score is 1, whereas the worst value is 0.
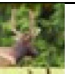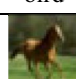
Dataset

In order to illustrate the effectiveness of our proposed method, we evaluated the performance of our method on three different datasets, as described in detail below. Samples of the three datasets are illustrated in Fig. 4.

CIFAR-10 This dataset collected by Alex et al. is a dataset for image recognition. The dataset has 60,000 32×32 color images, including 50,000 training data and 10,000 testing data. These data are divided into 10 categories, namely, aircraft, car, bird, cat, deer, dog, frog, horse, boat, and truck. In the experiments, one of the categories was randomly chosen as abnormal and the rest as normal. Following this way can yield 10 different cases, and each contains 45,000 normal.

ILD This dataset is the popular ILD database publicly available from the University Hospital of Geneva [19], including 109 High Resolution CT of different ILDs. The evaluations

Fig. 4 Samples of the three datasets

of the CT were performed by at least three experienced radiologists. The popular research patterns contain 5 classes, namely, healthy tissue, ground glass, emphysema, fibrosis, and micronodules. In the experiments, healthy tissue was chosen as normal, and the random one of the others was selected as abnormal. Following this way, we can yield 4 different cases.

HAM10000 Human Against Machine with 10,000 training images (HAM10000) datasets, developed by Tschandl et al. [20], consists of 10,015 dermatoscopic image sample within different nationalities, different acquired and stored modalities. This database contains all important diagnostic classes in the field of pigmented lesions, which are divided into seven categories. The cases in this dataset have high imbalance. In this dataset, akiec, bcc, df, vasc were selected as the abnormal classes, since the case number within these classes is relatively smaller.

Parameter Setting

The parameters of the proposed architecture are given as follows:

The learning rate is 0.0002; the batch size is 64. The number of epochs is 50, and the dropout rate is 0.5. The parameters in Eq. (7) are set to $\lambda_s = 50$, $\lambda_{adv} = 1$, $\lambda_{lat} = 1$. The proposed model is implemented by using Pytorch (v1.3.1, Python 3.7.5, CUDA 10.2, and CUDNN 7.3.1). All the experiments are conducted by using an NVIDIA Titan V GPU.

Results and Discussions

Table 1 presents a comparison of the proposed approach with other methods such as AnoGAN [28], EGBAD [35], GANomaly [15], and Skip-GANomaly [17]. AnoGAN only adopts latent vector to detect anomaly, while EGBAD only adopts reconstructed image to detect anomaly. Unlike AnoGAN and EGBAD, GANomaly and Skip-GANomaly adopt latent vector and reconstructed image jointly to detect anomaly. In Fig. 5, it is obvious that our proposed method clearly outperforms the other methods in each anomaly class on the CIFAR-10 dataset. For the most challenging
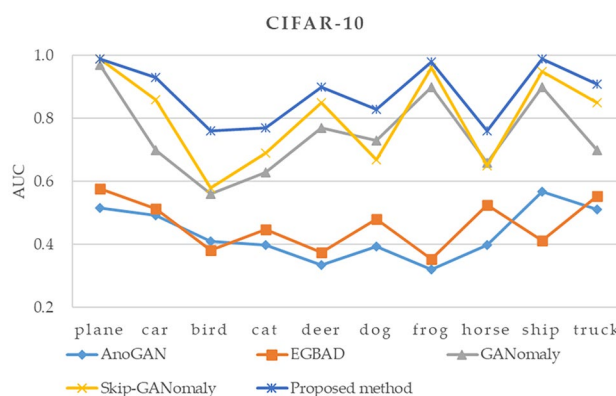

Fig. 5 A comparison of the obtained AUC results of different methods on the CIFAR-10 dataset

abnormality class like bird, the best AUC result of the rest model is 0.581, while our method achieves the AUC result of 0.758.

Tables 2 and 3 show the experimental results for ILD, and Tables 4 and 5 present the experimental results for HAM10000 datasets. It is clear that our approach obviously beats the other works in each anomaly class of the used datasets. The best ACC/F1-score of the previous work is 0.769/0.813 for the abnormality fibrosis class, whereas our method obtains the ACC/F1-score values as 0.952/0.954.

There are several possible reasons for other anomaly detection method that performed poorly on these datasets: (i) for a selected abnormal category, such as bird or dog, there exists a similar normal class such as plane or cat; (ii) the lesion features from samples of medical datasets, such as ILD and HAM10000, are small, without sufficient reconstructing capability that cannot capture small features in medical datasets.

The length of a CCB affects the performance of the proposed model. To evaluate the effectiveness of the length of the used CCB, in task 1 and task 2, the CCB length of each layer is 1,2,3,4 from bottom to top, and the performance of the proposed model was evaluated after doubling, tripling, and quadrupling the length in task 3. Tables 6 and 7 and Figs. 6 and 7 show the results of different length of the CCB for ILD and HAM10000. It is clear that with the increase of length of CCB, ACC

Table 1 The detailed AUC results of different methods on the CIFAR-10 dataset

CIFAR-10										
Model	Plane	Car	Bird	Cat	Deer	Dog	Frog	Horse	Ship	Truck
AnoGAN[28]	0.516	0.492	0.411	0.399	0.335	0.393	0.321	0.399	0.567	0.511
EGBAD[35]	0.577	0.514	0.383	0.448	0.374	0.481	0.353	0.526	0.413	0.555
GANomaly[15]	0.974	0.697	0.562	0.631	0.774	0.734	0.898	0.661	0.895	0.703
Skip-GANomaly[17]	0.989	0.862	0.581	0.686	0.847	0.667	0.961	0.657	0.951	0.851
Proposed method	0.991	0.933	0.758	0.771	0.901	0.832	0.977	0.762	0.985	0.912

Table 2 The obtained ACC results of different methods for ILD

ILD-ACC				
Method	Fibrosis	Micronodules	Emphysema	Ground
AnoGAN [28]	0.532	0.498	0.394	0.477
EGBAD [35]	0.603	0.467	0.488	0.541
GANomaly [15]	0.769	0.524	0.518	0.724
Skip-GANomaly [17]	0.634	0.541	0.533	0.798
Proposed method	0.952	0.555	0.799	0.963

Table 3 The obtained F1 results of different methods for ILD

ILD-F1				
Method	Fibrosis	Micronodules	Emphysema	Ground
AnoGAN [28]	0.578	0.566	0.467	0.578
EGBAD [35]	0.621	0.514	0.582	0.615
GANomaly [15]	0.813	0.675	0.674	0.775
Skip-GANomaly[17]	0.732	0.685	0.681	0.832
Proposed method	0.954	0.692	0.819	0.964

Table 4 The obtained ACC results of different methods for HAM10000

HAM10000-ACC				
Method	akiec	bcc	df	vasc
AnoGAN [28]	0.433	0.478	0.623	0.463
EGBAD [35]	0.556	0.557	0.518	0.529
GANomaly [15]	0.561	0.635	0.561	0.535
Skip-GANomaly [17]	0.638	0.954	0.878	0.894
Proposed method	0.705	0.973	0.909	0.912

Table 5 The obtained F1 results of different methods for HAM10000

HAM10000-F1				
Method	akiec	bcc	df	vasc
AnoGAN[28]	0.412	0.437	0.612	0.512
EGBAD[35]	0.443	0.536	0.581	0.599
GANomaly[15]	0.438	0.583	0.653	0.605
Skip- GANomaly[17]	0.674	0.953	0.886	0.904
Proposed method	0.725	0.972	0.913	0.918

Table 6 The obtained ACC results of different length of the used CCB for ILD and HAM10000

	ILD-ACC				HAM10000-ACC			
Length of a CCB	Fibrosis	Micronodules	Emphysema	Ground	akiec	bcc	df	vasc
[1–4]	0.952	0.555	0.799	0.963	0.705	0.973	0.909	0.912
[2, 4, 6, 8]	0.938	0.512	0.783	0.866	0.703	0.827	0.848	0.905
[4, 8, 12, 16]	0.942	0.561	0.776	0.87	0.67	0.844	0.791	0.877
[6, 12, 18, 24]	0.939	0.498	0.758	0.851	0.683	0.832	0.817	0.903
[8, 16, 24, 32]	0.935	0.488	0.743	0.81	0.65	0.834	0.757	0.859

Table 7 The obtained F1 results of different length of the used CCB for ILD and HAM10000

Length of a CCB	ILD-F1				HAM10000-F1			
	Fibrosis	Micronodules	Emphysema	Ground	akiec	bcc	df	vasc
[1–4]	0.954	0.692	0.819	0.964	0.725	0.972	0.913	0.918
[2, 4, 6, 8]	0.936	0.617	0.798	0.902	0.629	0.792	0.821	0.907
[4, 8, 12, 16]	0.941	0.688	0.786	0.853	0.581	0.817	0.747	0.857
[6, 12, 18, 24]	0.935	0.578	0.779	0.861	0.616	0.801	0.788	0.901
[8, 16, 24, 32]	0.923	0.565	0.75	0.829	0.604	0.804	0.723	0.859

Fig. 6 The obtained ACC results for different length of the used CCB for ILD and HAM10000
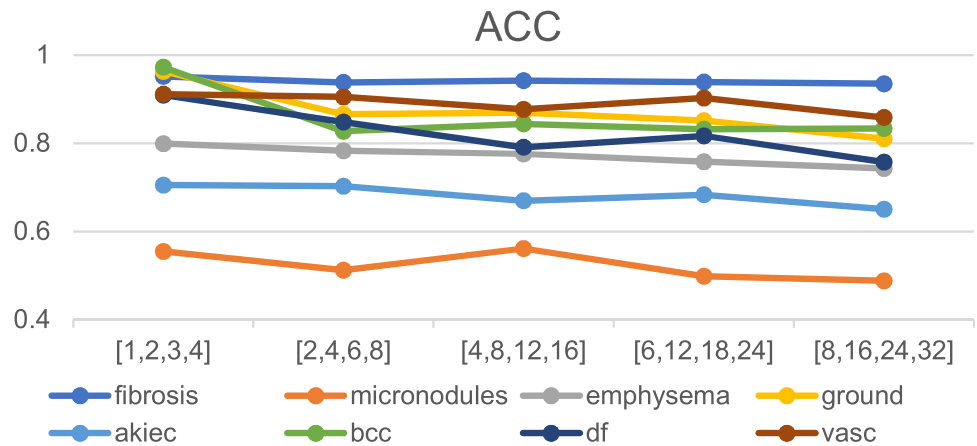
Fig. 7 The obtained F1 results for different length of the used CCB for ILD and HAM10000
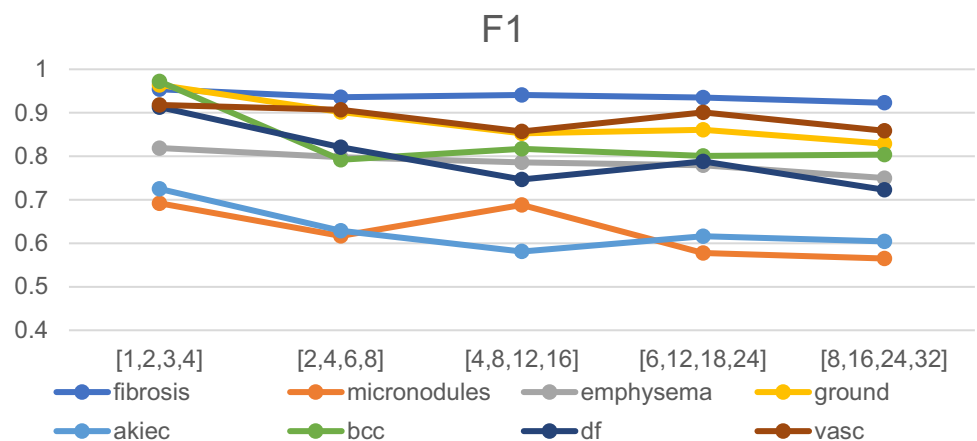
and F1 decreased slightly, and the best performance was obtained when the length was 1,2,3,4. The longer length will cause over fitting and affect the performance of the proposed model.

Conclusion

This paper proposes an unsupervised anomaly detection approach via an improved adversarial autoencoder, in which the conventional skip connections are replaced with a chain of convolution block (CCB). Our experimental results for multiple datasets (CIFAR-10, ILD, HAM10000) from different fields and complexity demonstrate that the proposed method presents superior performance to the state-of-the-art methods. Besides, the results indicate that the used CCB architecture provide more stable training. The empirical findings in task 2 give an insight into generality of our approach to different disease detection tasks. In future, our research will focus on the anomaly detection method containing temporal variation.

Author Contribution Conceptualization, H.Z. and W.G.; methodology, W.G. and H.Z.; software, H.Z.; validation, H.L., S.Z. and X.Z.; resources, X.Z.; writing–original draft preparation, W.G. and H.Z.;

Declarations

Competing Interests The authors declare no competing interests.

References

1. Agrawal R, Kulkarni S, Walambe R, Kotecha K: Assistive Framework for Automatic Detection of All the Zones in Retinopathy of Prematurity Using Deep Learning. J Digit Imaging, 2021
2. Feng-Ping A, Jun-e L, Jian-rong W: Medical image segmentation algorithm based on positive scaling invariant-self encoding CCA. Biomedical Signal Processing and Control 66:102395, 2021
3. Qiblawey Y, et al.: Detection and Severity Classification of COVID-19 in CT Images Using Deep Learning. Diagnostics (Basel) 11:893, 2021
4. Jojoa Acosta MF, Caballero Tovar LY, Garcia-Zapirain MB, Percybrooks WS: Melanoma diagnosis using deep learning techniques on dermatoscopic images. BMC Med Imaging 21:6, 2021
5. Jian C, et al.: Automatic brain extraction from 3D fetal MR image with deep learning-based multi-step framework. Comput Med Imaging Graph 88:101848, 2021
6. Muzamil S, Hussain T, Haider A, Waraich U, Ashiq U, Ayguade E: An Intelligent Iris Based Chronic Kidney Identification System. Symmetry-Basel 12:2066, 2020
7. Rehman MU, Cho S, Kim J, Chong KT: BrainSeg-Net: Brain Tumor MR Image Segmentation via Enhanced Encoder-Decoder Network. Diagnostics (Basel) 11:169, 2021
8. Nakao T, et al.: Unsupervised Deep Anomaly Detection in Chest Radiographs. J Digit Imaging 34:418-427, 2021
9. Baur C, Denner S, Wiestler B, Navab N, Albarqouni S: Autoencoders for unsupervised anomaly segmentation in brain MR images: A comparative study. Med Image Anal 69:101952, 2021
10. Fujioka T, et al.: Efficient Anomaly Detection with Generative Adversarial Network for Breast Ultrasound Imaging. Diagnostics (Basel) 10:456, 2020
11. Tufail AB, Ma YK, Zhang QN: Binary Classification of Alzheimer's Disease Using sMRI Imaging Modality and Deep Learning. J Digit Imaging 33:1073-1090, 2020
12. Park B, Park H, Lee SM, Seo JB, Kim N: Lung Segmentation on HRCT and Volumetric CT for Diffuse Interstitial Lung Disease Using Deep Convolutional Neural Networks. J Digit Imaging 32:1019-1026, 2019
13. Kim GB, et al.: Comparison of Shallow and Deep Learning Methods on Classifying the Regional Pattern of Diffuse Lung Disease. J Digit Imaging 31:415-424, 2018
14. Erfani SM, Rajasegarar S, Karunasekera S, Leckie C: High-dimensional and large-scale anomaly detection using a linear one-class SVM with deep learning. Pattern Recogn 58:121-134, 2016
15. Akcay S, Abarghouei AA, Breckon TP: GANomaly: Semi-supervised Anomaly Detection via Adversarial Training, 2018
16. Ibtehaz N, Rahman MS: MultiResUNet : Rethinking the U-Net architecture for multimodal biomedical image segmentation. Neural Netw 121:74-87, 2020
17. Akcay S, Atapour-Abarghouei A, Breckon TP: Skip-GANomaly: Skip Connected and Adversarially Trained Encoder-Decoder Anomaly Detection, 2019
18. Zenati H, Romain M, Foo C-S, Lecouat B, Chandrasekhar V: Adversarially Learned Anomaly Detection, 2018
19. Depeursinge A, Vargas A, Platon A, Geissbuhler A, Poletti PA, Muller H: Building a reference multimedia database for interstitial lung diseases. Comput Med Imaging Graph 36:227-238, 2012
20. Tschandl P, Rosendahl C, Kittler H: The HAM10000 dataset, a large collection of multi-source dermatoscopic images of common pigmented skin lesions. Sci Data 5:180161, 2018
21. Gribbestad M, Hassan MU, I AH, Sundli K: Health Monitoring of Air Compressors Using Reconstruction-Based Deep Learning for Anomaly Detection with Increased Transparency. Entropy (Basel) 23:83, 2021
22. Cowton J, Kyriazakis I, Plotz T, Bacardit J: A Combined Deep Learning GRU-Autoencoder for the Early Detection of Respiratory Disease in Pigs Using Multiple Environmental Sensors. Sensors (Basel) 18:2521, 2018
23. Petrick N, et al.: A primitive study on unsupervised anomaly detection with an autoencoder in emergency head CT volumes, 2018
24. Kingma D, Welling M: Auto-Encoding Variational Bayes. ICLR, 2013
25. Gunduz H: An efficient dimensionality reduction method using filter-based feature selection and variational autoencoders on Parkinson's disease classification. Biomedical Signal Processing and Control 66:102452, 2021
26. Saxena D, Cao J: Generative Adversarial Networks (GANs): Challenges, Solutions, and Future Directions. ACM Computing Surveys 54:1-42, 2021
27. Goodfellow IJ, et al.: Generative Adversarial Networks. CoRR abs/1406.2661, 2014
28. Schlegl T, Seeböck P, Waldstein SM, Schmidt-Erfurth U, Langs G: Unsupervised Anomaly Detection with Generative Adversarial Networks to Guide Marker Discovery, 2017
29. Radford A, Metz L, Chintala S: Unsupervised Representation Learning with Deep Convolutional Generative Adversarial Networks, 2016
30. Sabokrou M, Khalooei M, Fathy M, Adeli E: Adversarially Learned One-Class Classifier for Novelty Detection, 2018
31. Ronneberger O, Fischer P, Brox T: U-Net: Convolutional Networks for Biomedical Image Segmentation, 2015
32. Zongwei Z, Siddiquee MMR, Tajbakhsh N, Jianming L: UNet++: A Nested U-Net Architecture for Medical Image Segmentation, 2018
33. Wenping G, Zhuoming X, Haibo Z: Interstitial lung disease classification using improved DenseNet. Multimed Tools Appl 78:30615-30626, 2018 https://doi.org/10.1007/s11042-018-6535-y
34. Perera P, Patel VM: Learning Deep Features for One-Class Classification. IEEE Trans Image Process 28:5450-5463, 2019
35. Zenati H, Foo CS, Lecouat B, Manek G, Chandrasekhar VR: Efficient GAN-Based Anomaly Detection. CoRR abs/1802.06222, 2018